Chemical effects at metal/oxide interfaces studied by x-ray-absorption spectroscopy

T. J. Regan*
Department of Applied Physics, Stanford University, Stanford, California 94305

H. Ohldag, C. Stamm, F. Nolting,† J. Lüning, and J. Stöhr
Stanford Synchrotron Radiation Laboratory, P.O. Box 4349, Stanford, California 94309

R. L. White
Materials Science and Engineering Department, Stanford University, Stanford, California 94305
(Received 22 March 2001; revised manuscript received 27 June 2001; published 14 November 2001)

A chemical and magnetic characterization of ferromagnet/antiferromagnet interfaces is essential to understand the microscopic origins of exchange anisotropy and other magnetic phenomena. We have used high-resolution *L*-edge x-ray absorption spectroscopy (XAS), which is element specific and sensitive to chemical environment and spin orientation, to investigate the interface of antiferromagnetic oxides with ferromagnetic metals. Clear quantitative evidence of oxidation/reduction reactions at the as-grown metal/oxide interface is presented. *In situ*– and *ex situ*–grown samples of the form oxide (5–30 Å)/metal (1–10 Å), where oxide is either NiO or CoO and metal is either Fe, Co, or Ni, were studied by high-resolution XAS. For all samples, a metal(oxide) layer adjacent to an oxide(metal) layer was partially oxidized(reduced). Quantitative analysis of the spectra showed that one to two atomic layers on either side of the interface were oxidized/reduced. An elemental series of samples showed that the amount of oxidation/reduction was in accord with the difference in oxidation potentials of the adjacent cations, e.g., oxide layers were more strongly reduced by an iron metal layer than by cobalt or nickel metal layers. Annealing to temperatures, typically used to bias devices, was shown to significantly increase the amount of oxidation/reduction. The oxidation behavior of iron was shown to depend on the amount of oxygen available. Our results are believed to provide important information for the improved understanding of exchange anisotropy.

DOI: 10.1103/PhysRevB.64.214422 PACS number(s): 75.70.−i, 81.65.Mq, 82.80.Pv, 82.65.+r

I. INTRODUCTION

Exchange anisotropy—the unidirectional coupling of a ferromagnet (F) to an adjacent antiferromagnet (AF)—is of interest both technologically and academically. Technologically, magnetic disk-drive read heads incorporating exchange anisotropy are essential to the attainment of data densities beyond ~1 Gb/in^2 (the 1997 industry standard). Academically, 45 years after its discovery[1] and 22 years after it was proposed for use in magnetic sensors,[2] a fundamental description of exchange anisotropy remains elusive. Recent reviews[3,4] describe the current state of understanding of exchange anisotropy and explain why its investigation is difficult: ''In common with most other magnetic phenomena in which surface and/or interfacial properties are important, there exists no basic, generally applicable, predictive theory/model (of exchange anisotropy). The reason is that the essential behavior depends critically on the atomic-level chemical and spin structure at a buried interface.''[4] The importance of the ferromagnetic/antiferromagnetic interface to exchange anisotropy is a specific example of the importance of interfaces to a variety of magnetic phenomena. For example, the giant magnetoresistance effect, spin tunneling, and spin injection are phenomena to which the exact nature of the associated interface is crucial. Techniques that can distinguish interface from bulk properties, and furthermore study the interface with spatial resolution, are therefore expected to become increasingly important.[5]

Synchrotron-based x-ray absorption spectroscopy (XAS) is well suited to the investigation of exchange anisotropy and other interfacial magnetic phenomena. The surface and near-surface (~20 Å) sensitivity of XAS, coupled with its intrinsic elemental specificity, makes possible the study of both sides of a buried interface. As will become apparent below, the XAS signal is sensitive to the chemical state of the element, and therefore to any departures from a nominal configuration. The linear and circular polarization of synchrotron light enables one to study the spin configuration of both antiferromagnets and ferromagnets. The inherently local nature of x-ray spectroscopy enables XAS-based microscopy techniques to study interfaces with spatial resolution, thereby imaging AF and F domains and deducing their couplings.[6,7]

In this work, the interface sensitivity of x-ray absorption spectroscopy was used to obtain clear, quantitative evidence of oxidation/reduction reactions at as-grown metal/oxide interfaces. These results were obtained from a variety of samples, different in preparation method and in elemental constituents, and therefore are expected to be generally valid. Different elements are shown to have different degrees of reactivity, an anneal is shown to increase the amount of reaction, and the oxidation behavior of iron is shown to depend on the amount of oxygen available. The implications of our results for the understanding of exchange anisotropy are considered.

II. EXPERIMENT

A. Sandwich samples

The total-electron-yield (TEY) mode of XAS spectroscopy was chosen for its surface to near-surface sensitivity

(appropriate for studying a buried interface) and experimental convenience. Sample-layer thicknesses ranged from 1–30 Å, balancing adequate weighting of the interfacial region in the total signal, and adequate overall signal intensity. Throughout this paper, samples containing an interface between metal and oxide layers will be called ''sandwiches.'' Three different methods of sandwich sample preparation are described below.

A set of sandwich samples (*ex situ*–grown sandwiches) was prepared in a molecular beam epitaxy synthesis chamber at Stanford University. The sandwiches were of the form MgO (001)/oxide (10 Å)/metal (10 Å)/Ru (20 Å), where oxide is either NiO or CoO and metal is either Fe, Co, or Ni. A given element occurred in only one layer of any given sandwich, ensuring that the element specificity of XAS could be translated to layer specificity. The sandwiches were fabricated by electron-beam evaporation from pure-metal sources at a base pressure of 4×10^{-8} torr. The oxide and metal thickness was monitored during deposition by a quartz-crystal monitor, which had been calibrated by x-ray reflectivity analysis of previous samples. MgO substrates were degreased by an ultrasound soak in 1,1,1-trichloroethane, acetone, and methanol (20 min, twice per solvent), rinsed with isopropanol, and loaded into the chamber.[8] They were then heated to 600 °C in an atmosphere of 1×10^{-5} torr molecular oxygen for ~12 h to remove carbon deposits.[9] Oxide growth took place in a molecular (CoO) or electron-cyclotron-resonance activated[8] (NiO) oxygen atmosphere of approximately 1×10^{-5} torr. Oxides were grown at 300 °C at a typical rate of 0.3–0.5 Å/sec; the samples were then cooled to room temperature, and the metals were deposited at similar rates. Note that the metal/oxide interface was created at room temperature and never annealed, unless otherwise specified. Samples were capped with ruthenium to protect the metal from oxidation during transport to the synchrotron radiation facility. Reflection high-energy electron diffraction images of the MgO substrate prior to deposition, and of the (001) NiO and CoO oxides, confirmed clean, flat, and well-ordered surfaces. High-angle symmetric and asymmetric x-ray diffraction scans on thick samples confirmed the growth of single-phase epitaxial NiO and CoO (100).

The *ex situ*–grown sandwiches present two complications: limited base pressure during metal deposition and the presence of a capping layer. The growth chamber, optimized for growing complex oxides, did not attain a base pressure typically required for growing clean metal layers. Test samples of the form MgO/Ru (50 Å)/Fe or Co (10 Å)/Ru (20 Å) were analyzed to determine the extent of metal oxidation during growth. It was determined that for iron ~0.5 Å of metal was oxidized during growth; cobalt oxidation was less than 0.5 Å. The ruthenium capping layer was found to effectively prevent oxidation of the underlying metals, as indicated by repeated scans of pure-metal samples kept in air for a period of months. However, ruthenium has absorption structure underlying the *L*-edge region of the transition metals, which complicates spectrum normalization. A disadvantage of any capping layer is the reduced intensity of electron-yield signals from the layers below.

A second set of sandwiches (*in situ*–grown sandwiches) was prepared to confirm that any metal oxidation seen for the *ex situ*–grown sandwiches was the effect of proximity to an oxide. These samples were grown on silicon substrates dipped in hydrofluoric acid to remove any oxides before insertion into a preparation chamber. The samples were of the form Si/NiO(5–30 Å)/Fe(1–10 Å). The NiO was deposited in a molecular oxygen atmosphere of 1×10^{-6} torr in a preparation chamber. The samples were then transferred through a small aperture to the main chamber with a base pressure of about 1×10^{-10} torr for metal deposition and XAS analysis. Both nickel and iron were evaporated by electron-beam bombardment of pure metal sources at typical rates of 1 Å/min. Scans of the nickel and iron absorption edges were performed after deposition of each layer. The x-ray absorption as well as Auger measurements were used to estimate the layer thicknesses during growth. The Auger signal was independently calibrated against *ex situ* x-ray reflectivity measurements on test samples. We estimate error bars of about 20% for the nominal (unreacted) layer thicknesses. For these sandwiches the absence of a capping layer avoided the problems of an interfering absorption structure and signal reduction.

A third set of sandwiches (''single-crystal'' sandwiches) of the form NiO bulk single crystal/metal(2–10 Å), where metal=Fe or Co, was studied in conjunction with XAS microscopy experiments.[10] Nickel oxide single crystals (Mateck GmbH) were cleaved to expose the (001) surface and immediately introduced into the XAS analysis chamber. Thin layers of iron or cobalt were then deposited under ultrahigh vacuum conditions as described above.

B. Standard samples

Pure metal and oxide standard samples were prepared for each element. These standards consisted of a thicker (200–600 Å) film to enable x-ray diffraction analysis and to obtain bulklike XAS spectra. Standards grown *ex situ* were capped by 20 Å of ruthenium (Ni metal, NiO, CoO), 20 Å platinum (Fe_3O_4), or 30 Å CN_x (α-Fe_2O_3). Other standards (Fe metal, Co metal) were grown and analyzed *in situ*. An FeO standard sample was prepared *in situ* according to a recipe in the literature.[11] The shift of the L_3 peak intensity ΔL_3 (oxide L_3 maximum minus metal L_3 maximum) was experimentally determined and the following values were obtained: FeO, ~0 eV; Fe_3O_4, 1.4 eV; α-Fe_2O_3, 1.7 eV; CoO, −0.25 eV; NiO, 0.4 eV.

A thin NiO layer has a lower antiferromagnetic ordering temperature than a bulk specimen.[12] Since the XAS spectrum contains information about magnetic ordering, the spectrum of a thin layer is different from the bulk spectrum. In addition, the thin-layer antiferromagnetic spin-axis orientation may differ from that of the bulk. Also, for thinner samples a possible reduction of the surface in vacuum will have a larger effect on the XAS spectrum that samples only the near-surface region. For these reasons, it is desirable to use a NiO standard of the same thickness as the NiO layer of the experimental sandwiches. Two thin NiO standards (5 Å and 30 Å, *in situ*–grown) were available and were employed in

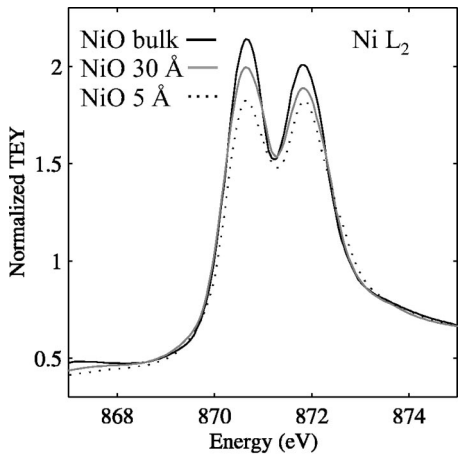

FIG. 1. Ni L_2 resonance XAS spectra of bulk (solid black), 30 Å (gray), and 5 Å (dotted black) nickel oxide standards. The multiplet (double-peak) structure is less defined for the thinner films. The spectra are normalized to zero before the L_3 peak and to an L-edge integrated intensity of 100 units.

the analysis where noted. The Ni L_2 resonance spectra of these thin standards, and the bulk NiO standard, are shown in Fig. 1; the multiplet peaks of the thinner layers are less defined.

C. XAS experiments

X-ray absorption spectroscopy experiments were performed on beamline 10-1 at the Stanford Synchrotron Radiation Laboratory. This wiggler/spherical grating monochromator beamline produces soft x rays in the range 200–1200 eV and we used an energy resolution of about 200 meV at 800 eV. A typical set of measurements included extended energy scans for identification of the major absorption edges and high-resolution scans over the L absorption edges of the oxide and metal layers. In order to accurately determine the relative energy positions of the L_3 and L_2 fine structure for the sandwiches and the corresponding standards we recorded sequential calibration spectra. We estimate the relative-energy accuracy of our sandwich and metal spectra to be about 50 meV. The absolute energy was calibrated by referencing our pure-metal spectra to those of Chen *et al.*[13] All scans were performed at normal incidence using linearly polarized light and in total-electron-yield mode. We simply measured the photocurrent of the samples with a picoammeter (typical signal 10^{-10} A), which was flux normalized by the photocurrent of a gold-grid reference monitor.[14]

III. ANALYSIS

A. Nominal and model sample structures

The nominal sandwich structure is illustrated in Fig. 2(a), where the layers are typically 10 Å thick and the capping layer and the substrate are omitted. In Fig. 2(b), discussed further in Sec. IV B, the regions that will take part in the interfacial reaction are noted with (i). Figure 2(c) illustrates a structure that would be the result of oxygen diffusion, driven by thermodynamic considerations, from a portion of the NiO

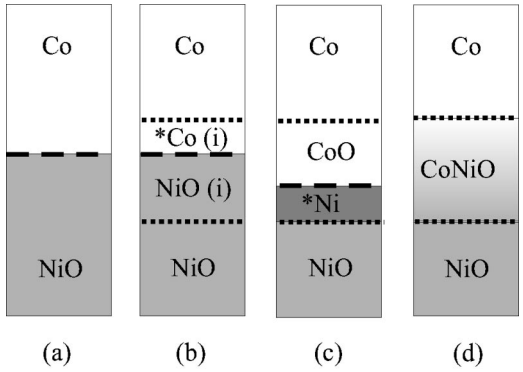

FIG. 2. Nominal sandwich sample structure and possible actual structures. Shading represents the concentration of nickel atoms. Part (a), the nominal structure, assumes an abrupt interface and no interface reactions; (b) describes the structure before the interfacial reaction, (i) denotes the regions that will take part in the reaction; (c), the model configuration for generation of test spectra, is the result of an interfacial reaction in which oxygen diffuses across the metal/oxide interface; (d) results from both oxygen and metal-ion diffusion, and assumes a graduated interface. The Ni-containing interfacial regions of (c) and (d) are possible sources for the interfacial uncompensated spin moments responsible for exchange anisotropy. The thicknesses of the starred metal regions of (b) and (c) are reported in Tables I, II, and III. The change of interface region thickness resulting from oxygen transfer is qualitatively represented in those figures.

to a portion of the Co. The darkness of the shading represents the concentration of nickel atoms. Figure 2(d) represents another possibility, the formation of a mixed Co-Ni-O compound at the interface region, and shows, via shading, a transition from nickel-rich to cobalt-rich. Such a structure would result from metal-ion and oxygen diffusion. Either of Figs. 2(c) and 2(d) would have implications for the study of exchange anisotropy, since the Ni-containing interfacial layers would be a source of uncompensated Ni moments [assuming formation of a ferrimagnetic alloy in Fig. 2(d)].

In this paper we will model the oxide/metal interface with the Fig. 2(c) structure, utilizing both the element specificity and the chemical sensitivity of the x-ray absorption technique. The former enables XAS to separately probe the Co and Ni containing layers in Fig. 2, the latter allows it to distinguish between metal and oxide components of the same element.

B. Analysis procedures

To describe our analysis procedure we will use the cobalt L-edge spectrum of the 10 Å CoO/10 Å Fe sandwich shown in Fig. 3. The plot shows the normalized experimental spectrum (solid black) and, for comparison, the normalized TEY spectra of pure cobalt metal (gray) and cobalt oxide (dotted black). Comparison of the CoO standard spectrum to the cobalt-edge spectrum of the CoO/Fe sandwich reveals three qualitative differences: relative to the pure oxide, the spectrum of CoO adjacent to Fe exhibits a decreased L_3 resonance intensity, an increase in intensity between the L_3 and

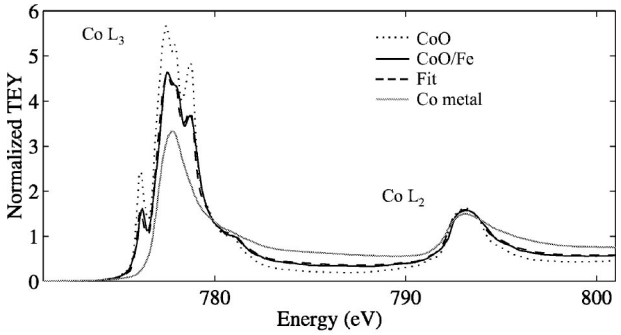

FIG. 3. Results of analysis procedure for the cobalt-edge spectrum of an *ex situ*–grown MgO(001)/CoO (10 Å)/Fe (10 Å)/Ru (20 Å) sandwich. Experimentally obtained total-electron-yield spectrum of the cobalt edge of the CoO/Fe sandwich, solid black. Best-fit model spectrum (2.2 Å of Co atop 6.1 Å of CoO) calculated via Eq. (A2) using CoO and Co parameters, dashed black. Pure Co metal standard TEY spectrum, gray; pure CoO standard TEY spectrum, dotted black. The experimentally obtained CoO/Fe spectrum has been normalized by subtracting an NiO/Fe reference spectrum and scaling to an *L*-edge integrated intensity of 100. The model spectrum and the metal and oxide standard spectra have been normalized by subtracting a linear pre-edge and scaling to an *L*-edge integrated intensity of 100.

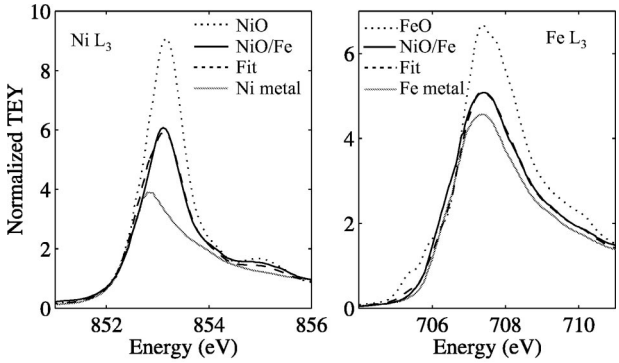

FIG. 4. Ni and Fe L_3 spectra of an *in situ*–grown NiO (5 Å)/Fe (5 Å) sandwich showing reduction of NiO and oxidation of Fe. Pure metal, gray; pure oxide, dotted black; sandwich-layer, solid black; best fit to sandwich-layer spectrum, dashed black. The fit to the Ni *L*-edge spectrum of the sandwich is of a model structure of 1.5 Å Ni atop 2.5 Å NiO—at the interface, 2.5 Å NiO has been reduced to Ni. The fit to the Fe *L*-edge spectrum of the sandwich is of a model structure of 3.4 Å Fe atop 2.9 Å FeO—at the interface, 1.6 Å Fe has been oxidized to FeO.

L_2 resonances, and a lessening of the L_3 multiplet definition (Appendix B, Sec. 2). These differences were noted for all samples studied and are believed to be a general characteristic of oxide reduction (or, expressed in reverse, of metal oxidation).

The best-fitting model spectrum (dashed black) in Fig. 3 was derived as follows. The nominally CoO layer was assumed to be of the form (x Å Co atop y Å CoO), with x and y to be determined. Model spectra of this cobalt-containing bilayer were calculated via Eq. (A2), using Co and CoO parameters, for various values of x and y (subject to the constraint Co^{2+} ions + Co metal atoms = constant). These model spectra were compared to the experimental CoO/Fe spectrum (black line), and it was determined that the experimental spectrum was best fit by the spectrum of the model bilayer ($x = 2.2$ Å Co atop $y = 6.1$ Å CoO). A separate analysis showed that the experimental iron *L*-edge spectrum was best fit by the spectrum of the model bilayer (7.1 Å Fe atop 5.3 Å iron oxide). Qualitatively, we conclude that oxygen diffusion from the nominally CoO layer to the nominally Fe layer has formed interfacial layers of cobalt metal and iron oxide.

The model and experimentally obtained TEY spectra were normalized prior to comparison, by subtraction of a linear background (or a suitable reference spectrum, if available) and overall scaling. For each model spectrum, the goodness of fit was calculated by simply summing the squares of the difference between the model datum and actual datum at each energy point, and dividing by the number of points. Typically, a separate best fit was identified for three energy regions: the L_3 resonance, the L_2 resonance, and the region between L_3 and L_2 (the interpeak region). The reported thicknesses were either an average of the results from the three regions (if within 20%), or the result from the region judged to be least affected by background or other uncertainties.

IV. RESULTS

A. Summary of results

At an as-grown metal/oxide interface, an interfacial reaction occurs that on one side of the interface oxidizes up to two atomic layers of metal, and on the other side of the interface produces up to two atomic layers of metal from oxide reduction. An anneal increases the amount of oxide reduction, and the relative reaction extent of different elemental combinations is in accord with thermodynamic considerations. Oxidation of cobalt and nickel can be modeled with the monoxide only, whereas oxidation of iron produces a mix of oxides dependent on the amount of oxygen available (Secs. IV B and IV D).

Figure 4 shows, for example, the L_3 resonances of nickel and iron for an *in situ*–grown NiO (5 Å)/Fe (5 Å) sandwich. Considering first the Ni L_3 resonance (left-hand plot), the spectrum of NiO adjacent to Fe (solid black) is in between the spectra of pure NiO (dotted black) and pure Ni metal (gray). This shows that the nominally pure NiO layer is in fact a mixture of nickel oxide and nickel metal. Similarly, the right-hand plot (Fe L_3 resonance) shows that the spectrum of Fe adjacent to NiO (solid black) is in between the spectra of pure iron metal (gray) and pure FeO (dotted black), showing that the nominally pure iron layer is in fact a mixture of Fe and FeO. Each plot displays a fit spectrum (dashed black) that quantifies the mixtures: the sandwich is best modeled as NiO (2.5 Å)/Ni (1.5 Å)/FeO (2.9 Å)/Fe (3.4 Å).

The oxidation/reduction reaction occurs at interfaces created at room temperature. To determine the effect of annealing, one sandwich [*ex situ*–grown MgO (001)/NiO

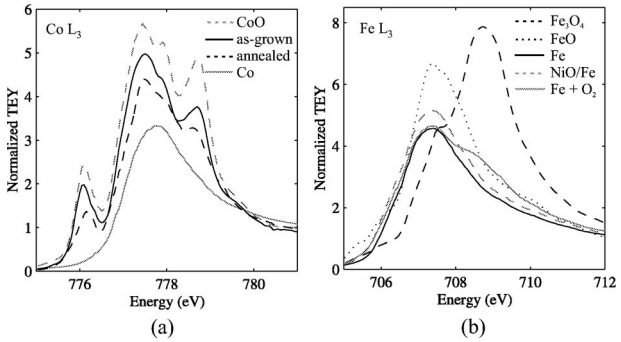

FIG. 5. Plot (a): Cobalt L_3-edge XAS spectra of an *ex situ*–grown MgO(001)/NiO (600 Å)/CoO (10 Å)/Fe (15 Å)/Ru (15 Å) sandwich showing the increased CoO reduction caused by annealing. Pure Co metal, solid gray; pure CoO, dashed gray; as-grown CoO/Fe, black; CoO/Fe after a 1 h, 230 °C anneal, dashed black. The increased reduction of CoO after the anneal is evident in the lessening of the multiplet-structure definition and in the overall decrease of the L_3 peak height. The anneal increases by 1 Å the amount of Co metal produced by oxide reduction. Plot (b): Differing oxidation behaviors of iron films. *In situ*–grown NiO/Fe, dashed gray; *in situ*–grown Fe with subsequent oxygen dosing (65 L shown), solid gray; Fe metal, black; FeO, dotted black; Fe_3O_4, dashed black. The NiO/Fe spectrum represents a limited-oxygen situation—oxygen only available from the adjacent NiO film. The lowest oxide of iron, FeO, is the result. The higher oxides of iron, represented here by Fe_3O_4, are formed when larger amounts of oxygen are available. The peak at ~709 eV (visible as a strong shoulder in the post-oxidized Fe spectrum) signals the presence of the higher oxides of iron.

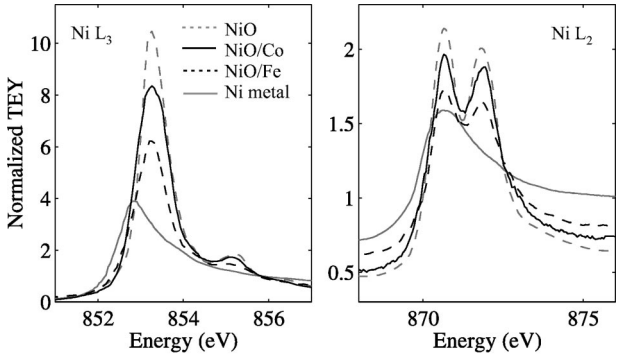

FIG. 6. Nickel L_3 and L_2 resonance spectra for Ni, NiO, and *ex situ*–grown MgO (001)/NiO (10 Å)/Fe or Co(10 Å)/Ru (20 Å) sandwiches, showing the reduction of nickel oxide by the adjacent metal. Ni metal, dark gray; NiO, dashed gray; NiO/Fe, dashed black; NiO/Co, solid black. Relative to pure nickel oxide, NiO adjacent to both Co and Fe has a lower L_3 peak intensity (left-hand plot), higher intensity between L_3 and L_2 (below 870 eV in the right-hand plot), and less multiplet definition (L_2 peak in the right-hand plot). These differences indicate reduction of the nominally nickel oxide layer by the adjacent metal. The spectrum of NiO adjacent to iron is more metallic than that of NiO adjacent to cobalt, showing that the NiO/Fe interface reacts more than the NiO/Co interface.

(600 Å)/CoO (10 Å)/Fe (15 Å)/Ru (15 Å)] was measured before and after a 1 h, 230 °C anneal. Figure 5 (a) displays the cobalt L_3 resonance for the sandwich sample before (solid black) and after (dashed black) the anneal, in addition to the spectra of pure CoO (dashed gray) and Co metal (solid gray) standard samples. The decrease of overall resonance height and the loss of definition of the multiplet structure of the resonance, relative to pure CoO, shows that the CoO layer adjacent to Fe was somewhat reduced as-grown, and was additionally reduced by the anneal. This anneal, typical of that employed in magnetic-device fabrication, increased the amount of cobalt metal (reduced cobalt oxide) by about 1 Å.

An elemental trend in reaction extent is evident from Fig. 6, which compares the spectrum of NiO adjacent to Co (solid black) to the spectrum of NiO adjacent to Fe (dashed black). The spectra of pure NiO (dashed gray) and pure Ni metal (solid gray) are included for reference. Oxide reduction (increase of metallic character) is indicated by a decrease of resonance height (at both the Ni L_3 and L_2 resonances) and loss of definition of multiplet structure (at the Ni L_2 resonance), relative to the pure NiO spectrum. The spectrum of NiO adjacent to iron is more metallic than that of NiO adjacent to cobalt, showing that the NiO/Fe interface reacts more than the NiO/Co interface.

In addition to the resonance height and multiplet structure, Fig. 6 displays a portion of the interpeak region (right-hand plot, energies $\leqslant$870 eV). In this region, the spectra of NiO adjacent to metal are higher than the pure oxide spectrum (and the effect is greater for NiO/Fe than for NiO/Co in accord with the elemental trends in reaction extent mentioned previously). The fact that the three spectral features—resonance height, interpeak height, and multiplet definition—tell the same story gives us confidence that the observed effect (oxide reduction in this case) is real, and not due to normalization or analysis procedures.

B. Tabulated results

Tables I–III present the results of the analysis procedure. In principle, for each sample, four best thicknesses could be reported: the thicknesses of the interfacial regions that will react [Co (i) and NiO (i) in Fig. 2(b)] and the thicknesses of the interfacial regions resulting from the reaction [CoO and Ni in drawing Fig. 2(c)]. We will report the two metal thicknesses: the thickness of metal that *results from* oxide reduction and the thickness of metal that *becomes* oxidized; the corresponding regions are starred in Fig. 2. If the final configuration of the sandwich is desired, the latter quantity can be converted to an oxide thickness. Via the appropriate molecular weights and densities, it is found that 1 Å of iron corresponds to 1.78 Å FeO, 2.11 Å Fe_3O_4, and 2.14 Å α-Fe_2O_3; 1 Å Co corresponds to 1.75 Å CoO; 1 Å Ni corresponds to 1.69 Å NiO.

The tables report all results with a relative precision of $\pm$0.1 Å. In practice, spectra differing by 0.1 Å in amount of metal component could be clearly distinguished only for the thinnest layers, i.e., the 1–3.5 Å Fe layers of Table I. For thicker layers, changes (in amount of metal) of 0.5 Å

TABLE I. Oxidation/reduction of *in situ*–prepared sandwiches consisting of either 5 or 30 Å NiO plus successive depositions of Fe. Entries represent either the thickness of Ni that results from NiO reduction, or the thickness of Fe that is oxidized to FeO.

Sandwich (grown *in situ*)			Amount reacted (Å)	
			Ni from NiO	Fe to FeO
30 Å NiO	+	1 Å Fe	1.2	0.7
	+	2 Å Fe	1.7	0.8
	+	3.5 Å Fe	2.6	0.9
5 Å NiO	+	5 Å Fe	1.5	1.6
	+	10 Å Fe	2.0	1.5

could be resolved. The effect of various sources of error on the reported results has been calculated.[15] It is found that, for example, using $\lambda_{NiO}=40$ Å (rather than 30 Å) increases the L_3-region analysis result (Ni layer thickness) by 1 Å. Subtracting a linear background rather than a reference-spectrum background can change the reported result by 1 Å. In summary, the experimental and analysis methods described in this work are sensitive to relative interfacial metal-layer thickness changes of 0.1 Å. A reasonable error bar for the absolute thicknesses reported in this work is 1 Å or one-half monolayer of interfacial metal.

Table I displays the extent of oxidation and reduction of *in situ*–grown NiO/Fe sandwiches. In analysis of the nickel-edge spectra we used the 30 Å or 5 Å NiO standard, as appropriate. For very thin iron layers deposited on NiO (upper portion of Table I) it is evident that deposition of additional iron increases the amount of interfacial reaction. For example, after deposition of 1 Å of Fe, NiO reduction produces 1.2 Å of Ni and 0.7 Å of Fe is oxidized to FeO. After deposition of an additional 1 Å of Fe (2 Å tabulated Fe thickness), the amount of nickel produced has increased to 1.7 Å and the amount of iron oxidized has increased to 0.8 Å. This demonstrates that the extent of reaction is limited by amount of reactant, for small quantities of reactant.

Table II summarizes the extent of oxidation/reduction for the *ex situ*–grown sandwiches. Elemental trends are evident.

TABLE II. Oxidation/reduction of *ex situ*–prepared sandwiches. Entries represent either the thickness of metal that results from oxide reduction, or the thickness of metal that is oxidized.

Sandwich (grown *ex situ*)			Amount reacted (Å)	
			Ni from NiO	Co to CoO
10 Å NiO	+	10 Å Co	1.4	2.2
			Co from CoO	Ni to NiO
10 Å CoO	+	10 Å Ni	1.3	1.0
			Ni from NiO	Fe to Fe_xO_y
10 Å NiO	+	10 Å Fe	3.2	3.3[a]
			Co from CoO	Fe to Fe_xO_y
10 Å CoO	+	10 Å Fe	2.2	2.9[b]

[a]3.0 Å Fe→FeO and 0.3 Å Fe→higher oxide (Fe_3O_4 or α-Fe_2O_3).
[b]2.4 Å Fe→FeO and 0.5 Å Fe→higher oxide.

TABLE III. Reduction of NiO single crystal (SC), and corresponding oxidation of metal, upon deposition of Co or Fe metal layers. Entries represent either the thickness of Ni that results from NiO reduction, or the thickness of cobalt or iron that is oxidized. The entry *x* means that the data was inadequate for analysis.

Sandwich (grown *in situ* on *ex situ*–cleaved NiO)			Amount reacted (Å)	
			Ni from NiO	Co to CoO
NiO SC	+	10 Å Co	0.7	0.9
			Ni from NiO	Fe to FeO
NiO SC	+	1.6 Å Fe	*x*	0.8
	+	3.4 Å Fe	1.4	1.0
	+	9.0 Å Fe	2.8	*x*

Iron metal is a stronger reducing agent than nickel or cobalt: a layer of iron adjacent to NiO produces (via reduction of NiO) 3.2 Å of Ni, whereas a layer of cobalt adjacent to NiO produces 1.4 Å of Ni. Also iron reduces nickel oxide (producing 3.2 Å Ni) more than it reduces cobalt oxide (producing 2.2 Å Co). Finally, the NiO/Co pair reacts somewhat more strongly than the CoO/Ni pair. These results are in qualitative agreement with thermodynamic considerations,[31] which predict that iron metal will be a significantly stronger, and cobalt metal a slightly stronger, reducing agent than nickel metal. In this *ex situ*–grown set of sandwiches, iron spectra were not expressible as a combination of the pure metal and the associated monoxide (FeO) only. The total amount of iron oxidized, listed in the table, was established from the interpeak region of the iron-edge spectrum, which is sensitive to ''amount of oxidation'' rather than to the specific oxide. The shape of the iron L_3 resonance showed that both the NiO/Fe and CoO/Fe sandwiches contained some iron atoms in environments characteristic of the higher oxides of iron,[32] and enabled an estimation of the amounts. Iron oxidation is discussed further in Sec. IV D.

Table III gives the oxidation/reduction results for the ''single-crystal'' sandwiches, which consist of layers of iron or cobalt deposited on *ex situ*–cleaved NiO (001). The single-crystal results are similar to those for the entirely *in situ*–grown sandwiches. At the cleaved NiO/metal interface, a thin layer of NiO reduces to nickel metal, and a thin layer of the metal is oxidized. Spectromicroscopy studies of a cleaved NiO/Co interface[16] identify the reduced-NiO layer as the origin of the interfacial spins crucial to exchange coupling.

C. Check of the oxygen-transfer hypothesis

We have modeled the interfacial reaction as a transfer of oxygen atoms across an abrupt interface. Therefore, the separate analyses of the metal and oxide layers of our sandwich samples should yield complementary results. This was qualitatively true for all samples, as demonstrated by Fig. 4, which shows that the reduction of NiO adjacent to Fe is accompanied by the expected iron oxidation. In principle, the oxygen-transfer hypothesis can be tested quantitatively by checking whether the amount of oxygen lost by the oxide

equals that gained by the metal. Keeping the number of oxygen atoms constant, consideration of the densities, molecular weights, and stoichiometries of the constituents predicts that 1 Å of Ni metal formed will correspond to 1.1/0.8/0.7 Å of Fe oxidized, if the iron oxide is respectively $FeO/Fe_3O_4/\alpha$-Fe_2O_3. The densities and molecular weights of both cobalt and nickel metal, and CoO and NiO, are nearly identical so a one-to-one relationship is expected in the case of CoO/Ni or NiO/Co sandwiches. Therefore it is expected that in Tables I and III, the iron entries will be 1.1 times the associated nickel entries. In Tables II and III, the cobalt entries should equal the nickel entries for the NiO/Co and CoO/Ni sandwiches. It is found, for example, that for the *ex situ*–grown CoO/Ni sandwich, 1.0 Å of nickel metal is oxidized to NiO, and 1.3 Å of cobalt metal results from reduction of CoO. However, since the absolute error bar ($\sim$1 Å) exceeds the difference between the Ni and Co values, the present experiment is not a quantitative test of the oxygen-transfer hypothesis.

D. Iron oxidation

Iron forms several stable oxides. Its oxidation behavior is therefore more complicated than that of nickel or cobalt. Figure 5(b), which shows the iron L_3-resonance spectra of two oxidized iron films, displays two different oxidation behaviors. The spectrum of *in situ*–grown Fe on NiO (dashed gray) is intermediate between Fe metal (solid black) and FeO (dotted black), showing that only the lowest oxide of iron was formed in this case. In a separate experiment, a thick iron layer was grown *in situ* and postoxidized by repeated doses of molecular oxygen. Shown (solid gray) is the spectrum after exposure to 65 L of O_2. The strong shoulder at $\sim$709 eV reveals the presence of a higher oxide, either Fe_3O_4 (dashed black) or α-Fe_2O_3 (not shown). The evolution with oxygen dose of the peak associated with Fe and FeO, at 707.36 eV, was particularly interesting. This peak initially increased, reached a maximum at 15 L O_2, and then decreased. The higher-oxide peak at $\sim$709 eV was evident as a shoulder after 35 L O_2 and thereafter increased. We conclude that the formation of the lowest oxide, the compound FeO, occurs only when oxygen is available in limited quantities. This was the case for the *in situ*–grown NiO/Fe: the only source of oxygen was the adjacent NiO layer. When oxygen is present in large quantities, the higher oxides are formed. The *ex situ*–grown MgO/NiO or CoO/Fe/Ru sandwiches were an intermediate case: oxygen was present in limited quantity at the NiO/Fe interface and in larger quantities during iron growth in the 4×10^{-8} base pressure.

V. DISCUSSION

A. Interface structure

In this section the assumptions underlying the Fig. 2(c) model structure will be evaluated. The first assumption, used in deduction of the thickness of the oxidized/reduced region, is that the border between reacted and unreacted material is abrupt. This is of course unlikely. Consider as an example a nominally pure metal layer adjacent to an oxide. We believe that one or at most two atomic layers adjacent to the interface are fully oxidized, the layers far (10 Å) from the interface are pure metal, and the region between these extremes transitions gradually from oxide-rich to metal-rich. This belief is supported by a recent study[17] that finds that when permalloy is deposited at 100 °C on γ-Fe_2O_3, the thickness of the resulting interfacial layer, measured by change in oxygen concentration, is $\sim$10 Å. The abruptness of the oxide-rich to metal-rich transition is governed by the interplay of thermodynamic forces and kinetic considerations.

A second assumption is that the resulting intermixed region can be described as a two-phase combination (of the pure metal and associated monoxide). This assumption resulted in satisfactory fits in almost all of the cases in this work. The exceptional cases—*ex situ*–grown iron layers, which contained several different iron oxides—have been noted in Sec. IV B. There is the further possibility that, if kinetic considerations preclude the attainment of thermodynamic equilibrium, an atom may be in a nonequilibrium oxide coordination. It may be difficult to establish a standard absorption spectrum in this case.

A third assumption is that the two reacted regions (reduced oxide and oxidized metal) remain distinct as shown in Fig. 2(c) rather than mix as shown in Fig. 2(d). In fact, there is experimental evidence that in some cases these two regions mix to form a single interfacial compound. For example, a Mössbauer spectroscopy study[18] of a CoO/Fe/Ni sample found a complicated mix of iron and iron/nickel environments. Determining the precise reaction mechanism or exact nature of the product formed is challenging, but some progress has been made: recent works have identified the product of reactions at a NiO/α-Fe_2O_3 (Ref. 19) or NiO/γ-Fe_2O_3 (Ref. 17) interface as nickel ferrite. To investigate this possibility using the methods of the present work, a standard spectrum of the interfacial species—Co_xNi_yO in the case of Fig. 2(d)—is needed.

B. Application of XAS to magnetic systems

This study has focused solely on the chemistry of the metal/oxide interface. An important additional capability of XAS is its sensitivity to magnetic ordering. The magnetic information is contained in the same multiplet structure that is a signature of the various chemical species—antiferromagnetic ordering, for example, is seen as an increase of some peaks, and a decrease of others, within a particular multiplet.[12] Therefore, extraction of magnetic information from XAS spectra of a complex system requires knowledge of both the chemical signatures of the component species, and the modifications of those signatures that accompany magnetic ordering. Once this information is known, XAS can determine the magnetic ordering not only of each *element*, but of different chemical *phases* of the same element. The present study is significant not only for its expected general applicability, but as a necessary foundation for the study of magnetic interfaces using XAS.

In particular, XAS is well suited to the study of exchange-biased interfaces. It has long been recognized that exchange anisotropy is an interface phenomenon that depends on the

existence of uncompensated interfacial spin moments. Much work has been devoted to finding the origin of these interfacial spins. The present work provides evidence that the interfacial spins are of chemical origin. More specifically, at the interface of an NiO/Co exchange-biased sandwich, there exists a nickel-metal-like (or ferrimagnetic Ni) region that is the source of the uncompensated interfacial spins. Such a model[20] of exchange anisotropy receives strong support from spectromicroscopic imaging of the spin moment of this interfacial layer.[16]

VI. CONCLUSION

The present study demonstrates the existence of chemical reactions at metal/oxide interfaces. Such an interface can be described as an oxidized-metal region adjacent to a reduced-oxide region. The metal regions involved (either oxide that has been reduced or metal that will be oxidized) are up to two atomic layers thick. The metal-like layer resulting from oxide reduction is a possible origin for the interfacial magnetic moments that give rise to coercivity increases and exchange anisotropy.

ACKNOWLEDGMENTS

We thank Robin Farrow at IBM-Almaden for supplying the Fe_3O_4 sample and Scott Chambers at the Pacific Northwest National Laboratory for supplying the α-Fe_2O_3 sample. T.J.R. thanks M. R. Beasley's group, Stanford University, for the use of, and assistance with, their MBE chamber, supported by AFOSR Grant No. F49620-98-1-0017. XAS measurements were performed at SSRL, which is operated by the Department of Energy, Office of Basic Energy Sciences. Support for this project was provided by NSF Grant No. ECS-9810185. The authors gratefully acknowledge assistance from SSRL staff, in particular the help of Stephen Sun with substrate preparation, and Nels Runsvick with equipment design and construction.

APPENDIX A: TOTAL ELECTRON YIELD SPECTRUM OF A BILAYER

In the following we derive an expression for the total-electron-yield x-ray absorption spectrum of a bilayer. We will treat the case of a partially reduced nickel oxide layer, modeled as a thin layer of nickel metal (reduced oxide) atop the remaining nickel oxide, as depicted in Fig. 2(c). The upper layer (Ni), thickness $t_{\mathrm{Ni}}=z_1$, extends from the surface ($z=0$) to depth z_1; the lower layer (NiO), thickness $t_{\mathrm{NiO}}=z_2-z_1$, extends from depth z_1 to z_2.

At normal x-ray incidence, the total electron yield dN_e from a nickel metal layer of thickness dz at a depth z is given by[21]

$$dN_{e,\mathrm{Ni}}=I_0\, e^{-z\mu_{\mathrm{Ni}}(E)}\mu_{\mathrm{Ni}}(E)G_{\mathrm{Ni}}(E)e^{-z/\lambda_{\mathrm{Ni}}}\,dz. \quad \text{(A1)}$$

Here I_0 is the number of photons striking the sample surface, $\mu_{\mathrm{Ni}}(E)$ is the absorption coefficient representing the probability of photon absorption [the x-ray absorption length is $1/\mu(E)$], and $G_{\mathrm{Ni}}(E)$ is the number of electrons produced per absorbed photon. The first exponential denotes the probability of a photon penetrating to depth z, and the second exponential denotes the probability of an electron created at depth z escaping from the sample. The quantity λ_{Ni} is the electron escape depth.

Integration of Eq. (A1) leads to the well-known expression for the total electron yield of a single layer (here, the nickel metal layer):

$$N_{e,\mathrm{Ni}}=I_0\frac{G_{\mathrm{Ni}}(E)}{1+\dfrac{1}{\mu_{\mathrm{Ni}}(E)\,\lambda_{\mathrm{Ni}}}}(1-e^{-t_{\mathrm{Ni}}[\mu_{\mathrm{Ni}}(E)+1/\lambda_{\mathrm{Ni}}]}).$$

To obtain an expression for the signal from the underlying NiO, Eq. (A1) must be modified to account for the effect of the Ni overlayer. The appropriate differential expression is

$$dN_{e,\mathrm{NiO}}=I_0\, e^{-z_1\mu_{\mathrm{Ni}}(E)}e^{-(z-z_1)\mu_{\mathrm{NiO}}(E)}\mu_{\mathrm{NiO}}(E)G_{\mathrm{NiO}}(E)\times e^{-(z-z_1)/\lambda_{\mathrm{NiO}}}\,e^{-z_1/\lambda_{\mathrm{Ni}}}\,dz.$$

Terms have been added to account for the signal attenuation by the Ni layer, i.e., the reduction of the number of photons into and the number of electrons out of the NiO layer. The argument of the NiO exponentials, $(z-z_1)$, is the distance traveled in the NiO (at normal incidence).

After integration of the above expression over the NiO layer ($z=z_1$ to z_2) the total signal from the Ni/NiO bilayer can be formed:

$$N_{e,\mathrm{Ni}}+N_{e,\mathrm{NiO}}=I_0\left(\frac{G_{\mathrm{Ni}}(E)}{1+\dfrac{1}{\mu_{\mathrm{Ni}}(E)\,\lambda_{\mathrm{Ni}}}}(1-e^{-t_{\mathrm{Ni}}[\mu_{\mathrm{Ni}}(E)+1/\lambda_{\mathrm{Ni}}]})+e^{-t_{\mathrm{Ni}}[\mu_{\mathrm{Ni}}(E)+1/\lambda_{\mathrm{Ni}}]}\frac{G_{\mathrm{NiO}}(E)}{1+\dfrac{1}{\mu_{\mathrm{NiO}}(E)\,\lambda_{\mathrm{NiO}}}}\times(1-e^{-t_{\mathrm{NiO}}[\mu_{\mathrm{NiO}}(E)+1/\lambda_{\mathrm{NiO}}]})\right). \quad \text{(A2)}$$

The first term of Eq. (A2) is the Ni metal (upper layer) signal; the second term is the NiO (lower layer) signal, attenuated by the factor $e^{-t_{\mathrm{Ni}}[\mu_{\mathrm{Ni}}(E)+1/\lambda_{\mathrm{Ni}}]}$ representing the effect of the Ni metal layer.

Note that in the case of a sample such as that depicted in Fig. 2(c), the nickel-edge spectrum will contain in addition contributions from other absorbing species (e.g., Co and Ru). These contributions are assumed accounted for in background subtraction and are not represented in Eq. (A2).

Formalism for the many-layer case is developed in O'Brien and Tonner.[22]

APPENDIX B: DERIVATION AND DISCUSSION OF STANDARD SPECTRA

1. Derivation of standard absorption spectra from electron-yield spectra

Via Eq. (A2), the TEY XAS spectrum of a bilayer can be calculated from the absorption spectra μ(E). Experimentally

obtained absorption spectra were not available for all of the chemical species considered in this work. Tabulated values for $\mu(E)$ can be found in the literature[23] and on the Internet[33] for all common materials. However, these tabulations are based on *atomic* x-ray absorption cross sections. They do not describe the important spectral regions near absorption edges, which are dominated by chemical bonding effects, and are therefore not sufficient for this work. We constructed the required absorption spectra from TEY spectra of pure standard samples; since this procedure is not well established we outline it here.

The well-known expression for the TEY spectrum $N_e(E)$ of a semi-infinitely thick sample (such as our standard samples) is written in terms of the absorption spectrum $\mu(E)$ as[24,25]

$$N_e(E)=\mathcal{T}\left[\frac{\mu(E)}{1+\lambda\mu(E)}\right], \tag{B1a}$$

$$N_e(E)=\mathcal{T}\,[\mu(E)]. \tag{B1b}$$

The former equation describes the entire spectrum, including the absorption edges where saturation may be important. The latter equation describes only the pre-edge and postedge regions of the spectrum, where saturation effects can be neglected. The important portion of the transformation $\mathcal{T}\equiv I_0 G(E)\lambda$ is the term $G(E)$, which describes the conversion of absorbed photons into electrons.[14,26] We will assume that over a single absorption edge, i.e., a spectral range of about 150 eV, $G(E)$ can be represented adequately as a linear function of E, therefore $\mathcal{T}$ is linear. We will not distinguish between $G(E)$ of the metal and oxide(s). Equation (B1a) shows that construction of $\mu(E)$ from $N_e(E)$ requires a knowledge of $\mathcal{T}$ (actually the inverse tranformation $\mathcal{T}^{-1}$) and the electron escape depth λ.

The first step in the construction is to determine the transformation. Inversion of Eq. (B1b) to yield $\mu(E)=\mathcal{T}^{-1}[N_e(E)]$ shows that the absorption and total-electron-yield spectra are simply related by the transformation $\mathcal{T}^{-1}$ in the pre-edge and postedge (unsaturated) regions of the spectrum. This transformation is determined operationally by manipulating the TEY spectrum such that it overlays the tabulated off-resonance absorption-coefficient spectrum in these regions. The required linear manipulations—subtraction of a pre-edge background and scaling by a constant or energy-dependent factor—constitute $\mathcal{T}^{-1}$. The left-hand plot of Fig. 7 gives an example of the overlay of the renormalized electron-yield spectrum of Ni metal, referred to as the ''overlay spectrum,'' with the tabulated absorption-coefficient spectrum. It is apparent that identification of the best overlay (solid gray) on the (smooth) tabulated absorption-coefficient spectrum (dashed black) is complicated by the significant postedge extended x-ray absorption fine structure (EXAFS) in the measured spectrum.

The electron-yield overlay spectrum is an intermediary in the analysis since it still needs to be corrected for saturation effects; this correction is the second step in the construction. Equation (B1a), valid in all regions of the spectrum, is inverted to yield

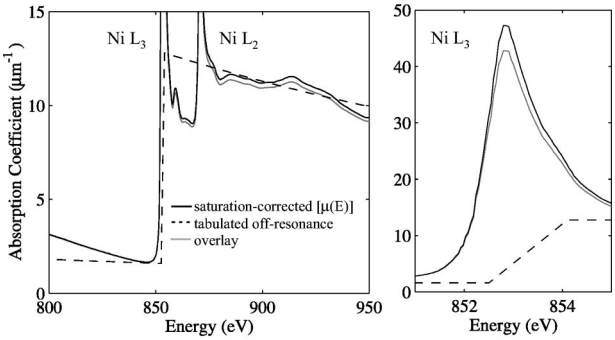

FIG. 7. Construction of absorption-coefficient spectrum from electron-yield spectrum. Tabulated absorption-coefficient spectrum, dashed black; overlay (saturated) electron-yield spectrum, gray; saturation-corrected (absorption coefficient) spectrum, solid black. Left-hand plot: pre-edge and postedge region of the nickel L edge, emphasizing the overlay of the electron-yield spectrum on the calculated off-resonance spectrum. Significant postedge (EXAFS) structure of the measured spectrum complicates identification of the best overlay. Right-hand plot: Ni L_3 region, emphasizing the correction for saturation. The higher of the two spectra is the (constructed) standard nickel metal absorption-coefficient spectrum. The lower of the two spectra is the overlaid electron-yield spectrum.

$$\mu(E)=\left(\frac{1}{\mathcal{T}^{-1}[N_e(E)]}-\lambda\right)^{-1}. \tag{B2}$$

The saturation-corrected spectrum $\mu(E)$ is determined by choosing a value for λ and performing the operations of Eq. (B2) on the overlay spectrum $\mathcal{T}^{-1}[N_e(E)]$. Here [and in Eq. (A2)] we have used electron escape depths from the literature: Fe, 15 Å (Refs. 21,27); Fe_3O_4, 50 Å (Ref. 28); α-Fe_2O_3, 35 Å (Ref. 28); Co, 22 Å (Refs. 27,25); Ni, 22 Å (Refs. 25,27). To our knowledge, the monoxide (FeO, CoO, NiO) electron escape depths have not been determined and we shall use a value of 30 Å. The result, the saturation-corrected overlay spectrum that corresponds to the absorption-coefficient spectrum $\mu(E)$, is shown (solid black) in the right-hand plot of Fig. 7 along with the overlay spectrum (solid gray) to display the effects of saturation. This procedure was performed on electron-yield spectra of the standard samples to yield the metal and oxide standard absorption spectra used in Eq. (A2).

In summary, deriving the absorption-coefficient spectrum from the electron-yield spectrum requires two steps. First, the electron-yield spectrum is overlaid on tabulated off-resonance absorption spectra, and second, the overlay spectrum is corrected for saturation effects. Related procedures have been described previously by Hunter Dunn *et al.*[24] and Gota *et al.*[28]

2. The standard spectra

Absorption spectra of pure metal and oxide standard samples are the foundation of quantitative analysis of bilayer XAS spectra. Appropriately normalized total-electron-yield

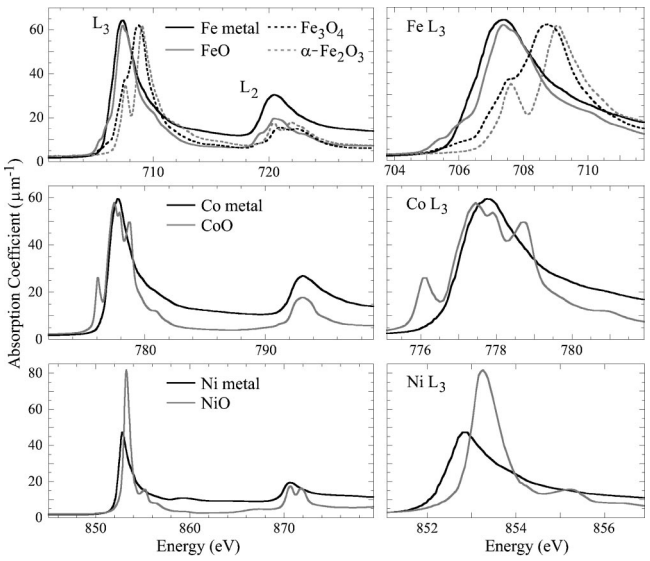

FIG. 8. Absolute absorption coefficient standard spectra for iron, cobalt, and nickel metals and oxides. Upper plots: Fe metal, solid black; FeO, solid gray; Fe_3O_4, dashed black; α-Fe_2O_3, dashed gray. Middle plots: Co metal, black; CoO, gray. Lower plots: Ni metal, black; NiO, gray. The L absorption edge ($2p \rightarrow 3d$ transition) is shown. The absolute absorption coefficient, units ($1/\mu$m), is the reciprocal of the photon penetration length. Left-hand panels, L_3 and L_2 regions; right-hand panels, expanded L_3 regions. The L_3 region displays the multiplet structure that is a fingerprint of the oxide.

spectra, while not suitable for quantitative analysis, are useful for recognition of oxidation or reduction effects. Here the standard spectra are presented and discussed.

Figure 8 displays the standard absorption spectra used in this work. The inherent element specificity of XAS is apparent, as the spectra for each element cover different energy ranges. The additional sensitivity to the chemical state of the absorbing atom (for example, an oxide environment) is manifested in the richer fine structure in the oxide spectra. The L_3 resonance of each compound is shown in the right-hand plots on an expanded scale. In general, the larger L_3 intensity for the oxides reflects their more-localized *d* bands, and the multiplet structure arising from crystal field and electron-electron correlation effects is unobscured by band-structure effects as discussed in detail by de Groot.[29] This has important implications for the application of XAS to magnetic systems, as is discussed in Sec. V B.

The TEY standard metal and oxide spectra shown in several figures were normalized as follows. A background was subtracted from the measured TEY spectra. We either subtracted a linear background or, when available, a background that included the EXAFS structure from lower-energy edges, measured on suitably prepared samples. The background-subtracted electron-yield spectrum has zero intensity below the absorption edge and can be conveniently rescaled. A common practice has been to scale spectra to a constant edge jump.[14,24] This procedure normalizes spectra to the same relative number of absorbing atoms. It requires spectra that extend to energies well above the edge where the spectra become smooth and a linear step function can be fitted. We have used here a different procedure justified by an empirical sum rule that states that for a given element the x-ray absorption intensity, integrated from below the edge to an energy of about 100 eV above the edge is remarkably constant, independent of sample orientation and chemical structure.[30] Such a normalization to constant intensity is less sensitive to differences in spectral shape than the normalization to a constant edge jump. For the electron-yield spectra in this paper we have chosen an integration interval 100 eV above the edge and have set the integrated intensity arbitrarily to a value of 100.

The standard metal and oxide TEY and (derived) absorption spectra are available from the authors upon request.

*Email address: tom.regan@kla-tencor.com
†Present address: Paul Scherrer Institute, Swiss Light Source, 5232 Villigen, Switzerland.

[1] W.H. Meiklejohn and C.P. Bean, Phys. Rev. **102**, 1413 (1956).
[2] R.D. Hempstead, S. Krongelb, and D.A. Thompson, IEEE Trans. Magn. **14**, 521 (1978).
[3] J. Nogués and I.K. Schuller, J. Magn. Magn. Mater. **192**, 203 (1999).
[4] A.E. Berkowitz and K. Takano, J. Magn. Magn. Mater. **200**, 552 (1999).
[5] J.B. Kortright, D.D. Awschalom, J. Stöhr, S.D. Bader, Y.U. Idzerda, S.S.P. Parkin, I.K. Schuller, and H.-C. Siegmann, J. Magn. Magn. Mater. **207**, 7 (1999).
[6] A. Scholl, J. Stöhr, J. Lüning, J.W. Seo, J. Fompeyrine, H. Siegwart, J.-P. Locquet, F. Nolting, S. Anders, E.E. Fullerton, M.R. Scheinfein, and H.A. Padmore, Science **287**, 1014 (2000).
[7] F. Nolting, A. Scholl, J. Stöhr, J.W. Seo, J. Fompeyrine, H. Siegwart, J.P. Locquet, S. Anders, J. Lüning, E.E. Fullerton, M.F. Toney, and M.R. Scheinfein, Nature (London) **405**, 767 (2000).
[8] D.M. Lind, S.D. Berry, G. Chern, H. Mathias, and L.R. Testardi, Phys. Rev. B **45**, 1838 (1992).
[9] S.D. Peacor and T. Hibma, Surf. Sci. **301**, 11 (1994).
[10] H. Ohldag, A. Scholl, F. Nolting, S. Anders, F.U. Hillebrecht, and J. Stöhr, Phys. Rev. Lett. **86**, 2878 (2001).
[11] J.S. Corneille, J.W. He, and D.W. Goodman, Surf. Sci. **338**, 211 (1995).
[12] D. Alders, L.H. Tjeng, F.C. Voogt, T. Hibma, G.A. Sawatzky, C.T. Chen, J. Vogel, M. Sacchi, and S. Iacobucci, Phys. Rev. B **57**, 11 623 (1998).
[13] C.T. Chen, Y.U. Idzerda, H.-J. Lin, N.V. Smith, G. Meigs, E. Chaban, G.H. Ho, E. Pellegrin, and F. Sette, Phys. Rev. Lett. **75**, 152 (1995).
[14] J. Stöhr, *NEXAFS Spectroscopy*, Springer Series in Surface Sciences Vol. 25 (Springer, Heidelberg, 1992).
[15] T. J. Regan, Ph.D. dissertation, Stanford University, 2001.
[16] H. Ohldag, T.J. Regan, J. Stöhr, A. Scholl, F. Nolting, J. Lüning, C. Stamm, S. Anders, and R.L. White (unpublished).
[17] R.F.C. Farrow, M.J. Carey, R.F. Marks, P.M. Rice, and D.J.

Smith, Appl. Phys. Lett. **77**, 1191 (2000).
[18] K. Takano, F.T. Parker, and A.E. Berkowitz, J. Appl. Phys. **81**, 5262 (1997).
[19] N. Keller, M. Guyot, A. Das, M. Porte, and R. Krishnan, Solid State Commun. **105**, 333 (1998).
[20] F.T. Parker, K. Takano, and A.E. Berkowitz, Phys. Rev. B **61**, 866 (2000).
[21] R. Nakajima, Ph.D. dissertation, Stanford University, 1998.
[22] W.L. O'Brien and B.P. Tonner, Phys. Rev. B **50**, 12 672 (1994).
[23] B.L. Henke, E.M. Gullikson, and J.C. Davis, At. Data Nucl. Data Tables **54**, 181 (1993).
[24] J. Hunter Dunn, D. Arvanitis, N. Mårtensson, M. Tischer, F. May, M. Russo, and K. Baberschke, J. Phys.: Condens. Matter **7**, 1111 (1995).
[25] R. Nakajima, J. Stöhr, and Y.U. Idzerda, Phys. Rev. B **59**, 6421 (1999).
[26] H. Henneken, F. Scholze, and G. Ulm, J. Appl. Phys. **87**, 257 (2000).
[27] V. Chakarian, Y.U. Idzerda, and C.T. Chen, Phys. Rev. B **57**, 5312 (1998).
[28] S. Gota, M. Gautier-Soyer, and M. Sacchi, Phys. Rev. B **62**, 4187 (2000).
[29] F.M.F. de Groot, J. Electron Spectrosc. Relat. Phenom. **67**, 529 (1994).
[30] J. Stöhr *et al.* (unpublished).
[31] Standard Gibbs Free Energies of Formation (kJ/mol): FeO −58.1, CoO −51.5, NiO −50.6.
[32] Since the unit cells of Fe_3O_4 and α-Fe_2O_3 are larger than a few atomic layers, we distinguish between formation of the bonding environment characteristic of the oxide, and formation of the oxide itself.
[33] http://www-cxro.lbl.gov